Supplementary Information

Quantitative Comparison of Local Field Enhancement from Tip-Apex and Plasmonic Nanofocusing Excitation via Plasmon-Assisted Field Emission Resonances

Chenfang Lin,[*a] Jie Li,[a] Guoao Li,[a] Wenjie Luo,[a] Shuyi Liu,[b] Adnan Hammud,[c] Yang Xia,[a] Anlian Pan,[a,d] Martin Wolf,[e] Melanie Müller,[e] Takashi Kumagai[*f,g]

[a]*Key Laboratory for Micro-Nano Physics and Technology of Hunan Province, State Key Laboratory of Chemo/Biosensing and Chemometrics, Hunan Institute of Optoelectronic Integration, College of Materials Science and Engineering, Hunan University, 410082, Changsha, China.*

[b]*Wuhan National Laboratory for Optoelectronics, Huazhong University of Science and Technology, Wuhan, 430074 China*

[c]*Department of Inorganic Chemistry, Fritz Haber Institute of the Max Planck Society, Faradayweg 4-6, 14195 Berlin, Germany*

[d]*School of Physics and Electronics, Hunan Normal University, 410081, Changsha, China*

[e]*Department of Physical Chemistry, Fritz Haber Institute of the Max Planck Society, Faradayweg 4-6, 14195 Berlin, Germany*

[f]*Institute for Molecular Science, 38 NishigoNaka, Myodaiji, Okazaki 444-8585, Japan*

[g]*The Graduate University for Advanced Studies, SOKENDAI, Hayama, Kanagawa 240-0193, Japan*

*Corresponding authors: lincf@hnu.edu.cn; kuma@ims.ac.jp

1. Detail methods about the simulation and fabrication of the grooved pyramid tip

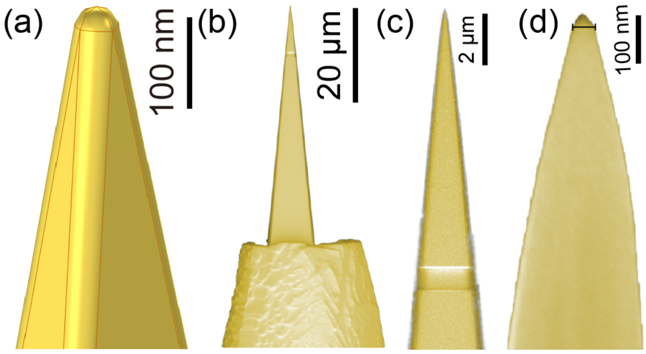

Fig. S1 (a) Geometric model of the tip apex used in the simulation.(b-d) false-color SEM images of the fabricated tip. The position at the tip apex with a diameter of 50 nm is marked by the horizontal bar.

Optimization of geometric parameters: The numerical simulation of the electromagnetic field is performed in COMSOL 6.1 based on the finite element method. The tip apex is modeled as a hemisphere with a diameter set to 50 nm (**Fig. S1d**). To ensure smooth connection between the apex sphere and the pyramidal shaft, the edges of the pyramid are rounded off with the same radius as that of the sphere at the apex (**Fig. S1a**). The complex refractive indices of Au and Ag are taken from Johnson and Christy.[1] The field enhancement at the very apex of the tip on the vacuum side is used for evaluation (**Fig. S2b**). The field distributions in the steady state are acquired by solving the time-harmonic wave equation. The scattered field is solved under a background field of an incident laser beam with a Gaussian-shaped electric-field profile, as shown in **Fig. S2a**. The incident beam is focused on the groove with its polarization (along the incident plane), angle (55°), and the focal spot diameter (6λ) chosen to match the experimental conditions (see also experimental part of methods in main text). To avoid artificial reflections, the pyramid is truncated by a sphere and surrounded by spherical perfectly matched layers. The mesh size is set to the default physics-controlled "extremely fine" configuration, and all results pass the mesh convergence test with an error of less than 1%.

Grooved tip fabrication: The grooved pyramidal tip was fabricated using focused ion beam (FIB) milling on an electrochemically etched Au tip with a Thermo Fisher FEI Helios NanoLab G3 FIB-SEM DualBeam system. This system provides gallium ions with energies up to 30 keV, enabling high-precision milling and deposition with critical dimensions below 10 nm. The pyramid shape and groove structure were formed by adjusting the tilt angles of the tip relative to the Ga^+ beam direction. To achieve efficient milling, high ion energies (30 keV) and beam currents (9.3 nA) were used, followed by lower-energy steps (5 keV and 2 keV) to the pyramid facets to minimize surface damage. The groove was shaped using a volume-per-dose parameter of 1.5 μm^3/nC for Au, with a low beam current of approximately 8 pA to prevent excessive milling and ensure precise groove depth.[2] Scanning electron microscope (SEM) images of the fabricated grooved pyramid-shaped Au tip are shown in **Fig. S1**(b–d).

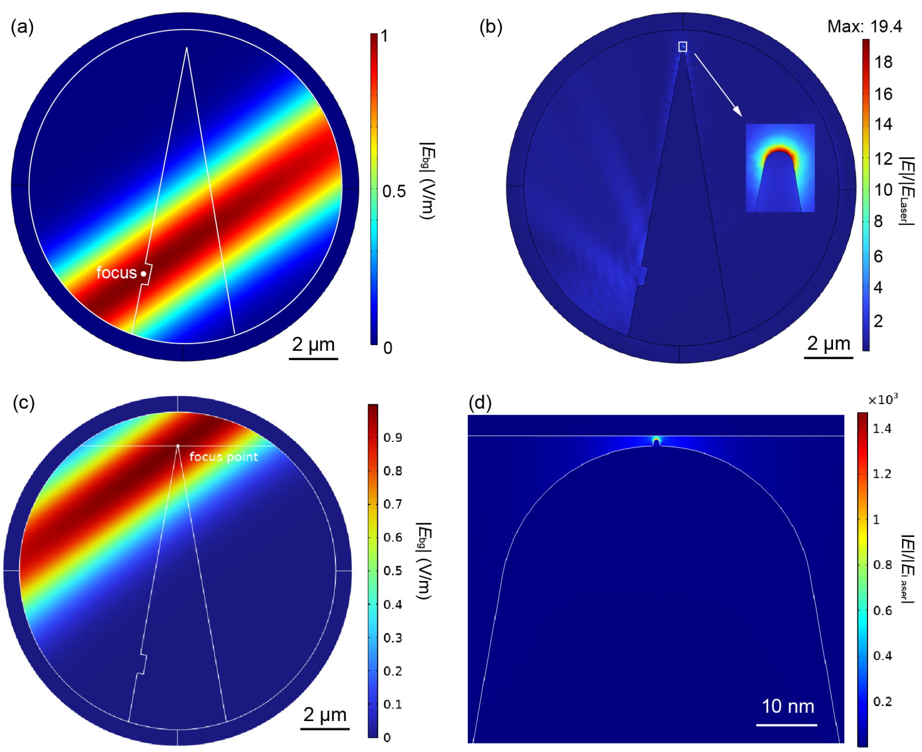

Fig. S2. Simulation structures and background field (E_{bg}) at the excitation wavelength of 780 nm. (a) (a) Background field of a Gaussian-profile incident laser beam. (b) Simulated field enhancement distribution for the selected structural parameters (W=900 nm, D=300 nm, θ_1=10° and θ_2=20°). The inset highlights the field enhancement distribution in the apex region. (c) Simulation structure of the STM junction and background field under apex illumination. (d) Simulated field enhancement distribution for the STM junction under groove illumination.

Simulations of field enhancement within the STM junction: We simulated the electric field enhancement distributions within the STM junction for both tip-apex and off-site excitation using the finite element method in COMSOL. The geometry of the STM junction consisting of the grooved tip and the Ag(111) sample is shown in **Fig. S2(c,d)**. The gap distance of the STM junction is set to 0.6 nm, which isa typical value for the tunneling setpoint of V=1 V and j=0.1 nA.[3] We considered two apex geometric structures, with and without an atomic-scale protrusion attached to the tip apex. The inclusion of such atomic-scale protrusions is crucial, as they generate extremely confined near-fields, making them essential for achieving exceptional sensitivity and resolution in tip-enhanced spectroscopy.[4,5] We modified the default physics-controlled "extremely fine" configuration to change the minimum element size to 1 nm and 0.2 nm for the tip apex without and with atomic protrusion, respectively. This ensures that the meshes accurately reproduce the STM junctions. The maximum element size was retained at the default value of 0.2 times the wavelength. The other simulation parameters were kept identical to those used in the simulation for the free-standing tip.

2. Tip displacement – bias voltage dependencies in constant current mode

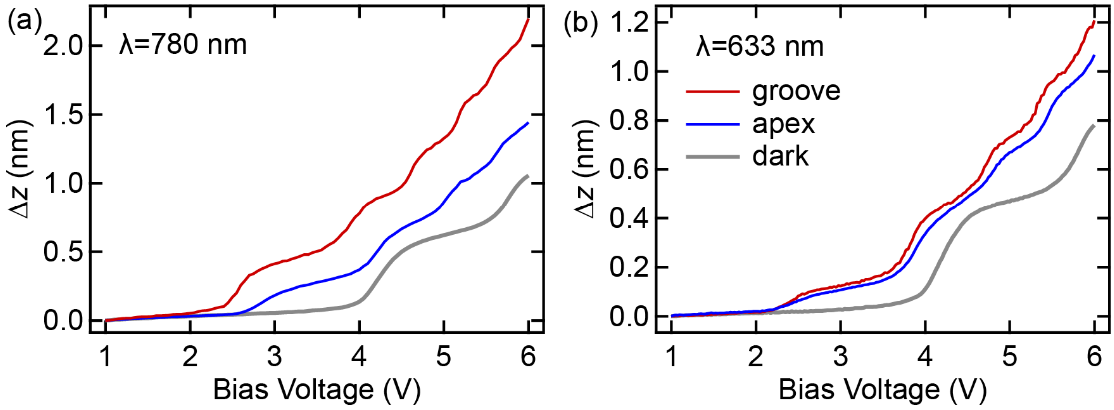

Fig. S3. The measured tip displacement (Δz) as a function of bias voltage in constant current mode (CCM). An increase in Δz corresponds to an increase in the gap distance. The excitation wavelengths are 780 nm in (a) and 633 nm in (b).

At V=1 V, the initial gap distance (d_0) is identical for all three curves, as it is set by the same tunneling conditions (V=1 V and j=0.1 nA). Under these conditions, the current is dominated by direct tunneling without photon assistance, making the photocurrent negligible (see ESI **Section 3** for details). At an excitation wavelength of 780 nm (**Fig. S3**a), due to the higher near-field intensity under groove illumination, the measured gap distances at the first plasmon-assisted field emission resonance (FER) peaks are higher under groove illumination (d_0+0.2 nm) than under apex illumination (d_0+0.09 nm). These differences in gap distance result in varying degrees of potential barrier distortion, leading to an energy shift in the image potential state.[6] Consequently, the first plasmon-assisted FER peak appears at different positions for groove and apex illumination.

In **Fig. 3**b of the main text (633-nm excitation), the first plasmon-assisted FER peak exhibits a slight shift of approximately 0.2 V between constant current mode (CCM) and constant-gap-distance mode (CGM). This shift is attributed to the energy variation of the image potential state due to differences in gap distance. In CGM, the gap distance remains constant, whereas in CCM, it increases with bias voltage (**Fig. S3**b). Consequently, the image potential state shifts slightly as the potential barrier in the gap is altered by the changing gap distance.[6]

3. Confirmation of negligible photocurrent at the tunneling setpoint of *V*=1 V and *j*=0.1 nA

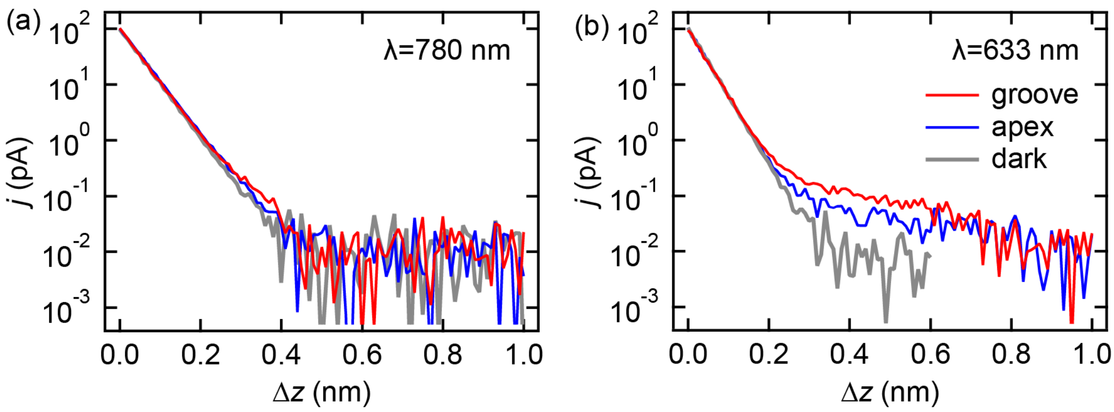

Fig. S4. Current (j) – tip displacement (Δz) curves under groove illumination, apex illumination, and in the absence of illumination (dark) at a bias voltage of 1 V. Panels (a) and (b) correspond to excitation wavelengths of 780 nm and 633 nm, respectively.

The identical slope in the tunneling regime ($\Delta z < 0.1$ nm) suggests that the majority of the current originates from electrons near the Fermi energy level.[3,7] Thus, at $\Delta z = 0$, the n-photon photocurrent is negligible, indicating that the gap distance set by the tunneling condition of V=1 V and j=0.1 nA remains consistent under both groove and apex illumination. At tip displacements between 0.2 nm and 0.6 nm, a two-photon photocurrent[3] (below 0.1 pA) begins to emerge at an excitation wavelength of 633 nm, but it does not affect the current at $\Delta z < 0.2$ nm.

4. Linear dependence of photocurrent on laser intensity

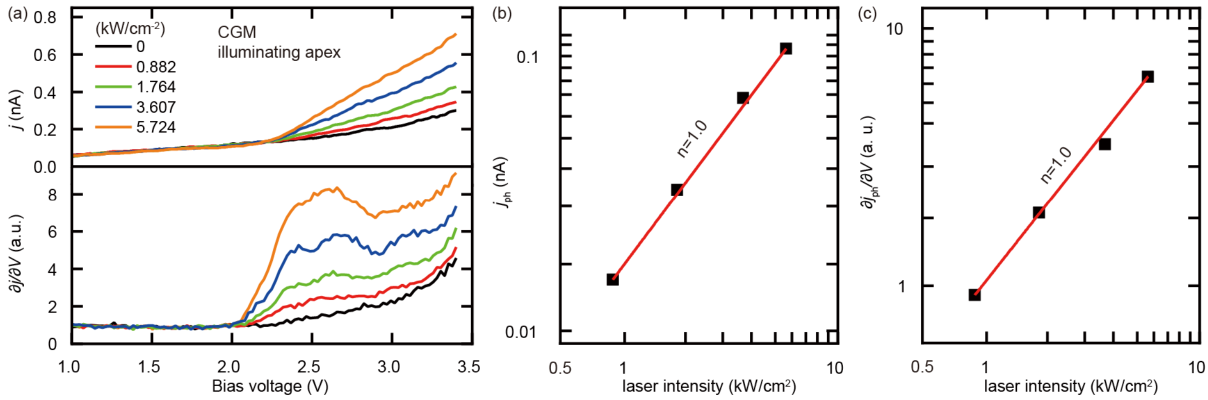

Fig. S5. (a) Current (j) and $\partial j/\partial V$ spectra in the constant-gap-distance mode (CGM) measured under apex illumination at an excitation wavelength of 633 nm for five different laser intensities (I_{laser}). (b–c) Photocurrent (j_{ph}) and $\partial j_{\text{ph}}/\partial V$ signal at $V = 2.5$ V plotted as a function of I_{laser}. The red lines represent power-law fittings based on $j_{\text{ph}} = I_{\text{Laser}}^{n}$, or $\frac{\partial j_{\text{ph}}}{\partial V} = I_{\text{Laser}}^{n}$, where n denotes the effective nonlinearity. An effective nonlinearity of ~1.0 is obtained for both j_{ph} and $\partial j_{\text{ph}}/\partial V$ signals, indicating a linear dependence of photocurrent and its derivative on laser intensity.

5. Ratio of the photocurrent under groove and apex illumination

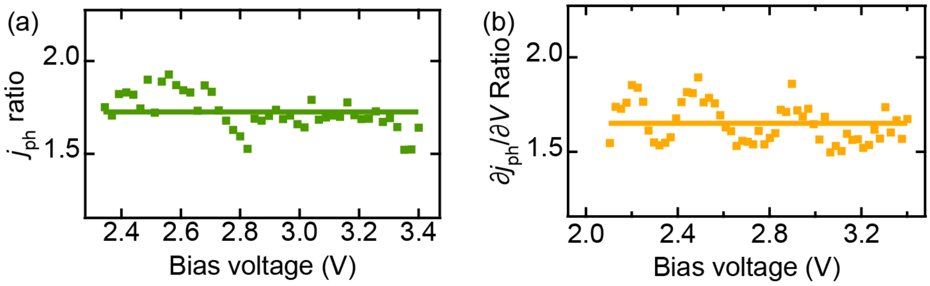

Fig. S6. Ratios of photocurrent (a) and $\partial j_{\mathrm{ph}}/\partial V$ (b) under groove and apex illumination as a function of bias voltage at an excitation wavelength of 633 nm. The horizontal lines indicate the average value.

From eqn (1) in the main text, we derive:

$$\frac{j_{\mathrm{ph}}\left(V,\left|E_{\mathrm{A}}^{\mathrm{iG}}\right|\right)}{j_{\mathrm{ph}}\left(V,\left|E_{\mathrm{A}}^{\mathrm{iA}}\right|\right)}=\frac{\left|E_{\mathrm{A}}^{\mathrm{iG}}\right|^2}{\left|E_{\mathrm{A}}^{\mathrm{iA}}\right|^2}. \tag{S1}$$

Thus, the photocurrent ratio under groove and apex illumination is equal to the ratio of $\frac{\partial j_{\mathrm{ph}}}{\partial V}$ and the ratio of local intensities, $\frac{\left|E_{\mathrm{A}}^{\mathrm{iG}}\right|^2}{\left|E_{\mathrm{A}}^{\mathrm{iA}}\right|^2}$, and remains independent of bias voltage. **Fig. S6** presents these ratios as a function of bias voltage. The photocurrent ratio does not exhibit the same oscillatory pattern as the $\partial j_{\mathrm{ph}}/\partial V$ ratio in **Fig. 3f** in the main text, suggesting that the observed oscillations in $\partial j_{\mathrm{ph}}/\partial V$ stem from noise in the lock-in amplifier. Furthermore, the average values of both ratios are comparable, confirming their validity.

References

1. P. B. Johnson and R. W. Christy, *Phys. Rev. B*, 1972, **6**, 4370-4379.
2. H. Bockmann, S. Liu, M. Muller, A. Hammud, M. Wolf and T. Kumagai, *Nano Lett.*, 2019, **19**, 3597-3602.
3. C. Lin, F. Krecinic, H. Yoshino, A. Hammud, A. Pan, M. Wolf, M. Müller and T. Kumagai, *ACS Photonics*, 2023, **10**, 3637-3646.
4. F. Benz, M. K. Schmidt, A. Dreismann, R. Chikkaraddy, Y. Zhang, A. Demetriadou, C. Carnegie, H. Ohadi, B. de Nijs, R. Esteban, J. Aizpurua and J. J. Baumberg, *Science*, 2016, **354**, 726-729.
5. B. Yang, G. Chen, A. Ghafoor, Y. Zhang, Y. Zhang, Y. Zhang, Y. Luo, J. Yang, V. Sandoghdar, J. Aizpurua, Z. Dong and J. G. Hou, *Nature Photonics*, 2020, **14**, 693-699.
6. T. Kumagai, S. Liu, A. Shiotari, D. Baugh, S. Shaikhutdinov and M. Wolf, *J Phys Condens Matter*, 2016, **28**, 494003.
7. B. Schröder, O. Bunjes, L. Wimmer, K. Kaiser, G. A. Traeger, T. Kotzott, C. Ropers and M. Wenderoth, *New Journal of Physics*, 2020, **22**, 033047.